 DOI: 10.1002/maco.201408215

KCl-induced high temperature corrosion of selected commercial alloys

Part II: alumina and silica-formers

S. Kiamehr*, K. V. Dahl, M. Montgomery and M. A. J. Somers

Laboratory testing on selected alumina and silica-forming alloys was performed to evaluate their performance against high temperature corrosion induced by potassium chloride (KCl). The alloys studied were FeCrAlY, Kanthal APM, Nimonic 80A, 214, 153MA and HR160. Exposure was conducted at 600 °C for 168 h in flowing N_2(g)+5%O_2(g)+15%H_2O(g) (vol.%) with samples covered under KCl powder. A KCl-free exposure was also performed for comparison. Corrosion morphology and products were studied with scanning electron microscopy (SEM), energy dispersive X-ray spectroscopy (EDS) and X-ray diffractometry (XRD). It was observed that alloying with aluminum did not lead to the formation of protective alumina for the studied alloys. The silicon containing stainless steel 153MA showed an analogous performance to low-silicon austenitic stainless steels of similar chromium and nickel contents. For alloy HR160, a potassium-chromium-silicon-oxygen containing layer forms as the innermost corrosion product. The layer was uniformly distributed over the surface and appears to render some protection as this alloy exhibited the best performance among the investigated alloys. To reveal further aspects of the corrosion mechanism, Nimonic 80A was exposed in static laboratory air for the same duration and temperature with either KCl or K_2CO_3 deposits. Comparison of results obtained with these experiments showed that both potassium and chlorine can play a role in material degradation by KCl.

1 Introduction

High temperature corrosion of heat exchangers due to potassium chloride (KCl) is a crucial factor in limiting the efficiency of power plants firing biomass. To keep the corrosion rates at an acceptable level, it is recommended that the outlet steam temperature does not exceed 540 °C [1], which reduces the efficiency of the plant. Therefore development of corrosion resistant materials has attracted much attention. The majority of high temperature alloys contain significant amounts of chromium to be able to form a chromium-rich oxide which protects against corrosion. However if the environment contains alkali elements, the initial oxide can be damaged due to alkali chromate formation [2]. To counteract such a problem, one solution could be to employ alloys with higher chromium content. However, several studies [3–5] show that increase in chromium content is not always a remedy against alkali chloride-induced high temperature corrosion. In fact, it has been demonstrated that if the temperature is high enough (above 500 °C) pure chromium is extremely reactive when exposed to alkali chlorides under oxidizing conditions [6–11]. Therefore the logical direction in materials selection is to employ other oxide-forming elements or improve the performance of chromia-forming alloys by addition of suitable alloying elements. There have been a number of investigations indicating that the presence of aluminum and/or silicon in Fe-Cr-(Ni) alloys is beneficial for corrosion resistance. For NaCl-induced attack in air under cyclic temperature conditions, *Hiramatsu* et al. [12] reported a better corrosion resistance with addition of aluminum in ferritic alloys and silicon in austenitic stainless steels. *Fujikawa* and *Maruyama* [13] investigated the effect of silicon content and aging on the high temperature corrosion of austenitic stainless steels exposed to NaCl in air. They reported a positive effect of silicon and a negative effect of aging due to the formation of chromium

S. Kiamehr, K. V. Dahl, M. Montgomery, M. A. J. Somers
Technical University of Denmark (DTU), Department of Mechanical Engineering, Produktionstorvet, Building 425 2800, Kgs. Lyngby, (Denmark)
E-mail: sabag@mek.dtu.dk

M. Montgomery
COWI A/S Parallelvej 2, 2800, Kgs. Lyngby, (Denmark)

Table 1. Chemical composition of the alloys. Carbon and nitrogen contents were measured with fusion thermal conductivity detection units LECO CS230 and LECO TN500, respectively. All values are in wt% (values in the parentheses are in at%). Elements without a value in the last column were present in trace amounts.

alloy	Fe	Cr	Ni	Al	Si	Mo	Co	Ti	C	N	other
FeCrAlY	bal.	23.2 (23.2)		5.1 (9.8)					0.040	0.018	Si,Ti, Zr
Kanthal APM	bal.	23.1 (22.9)		5.7 (10.9)	0.6 (1.1)				0.032	0.017	Ti,Zr
Nimonic 80A	0.8 (0.8)	20.7 (22.2)	bal.	1.4 (2.9)	0.4 (0.8)			2.3 (2.7)	0.070	0.014	
214	3.6 (3.5)	17.2 (18.0)	bal.	4.8 (9.7)					0.038	0.002	Zr
HR160	0.3 (0.3)	29.3 (30.8)	bal.		3.3 (6.5)	0.2 (0.1)	29.2 (27.1)	0.4 (0.5)	0.052	0.007	Al
153MA	bal.	20.4 (21.3)	10.0 (9.2)		1.6 (3.1)				0.048	0.15	Ce,La,Ti, Mn

carbides. *Li* et al. [14] studied the effect of aluminum and/or silicon addition to 9 wt% chromium steel P91 on its resistance against KCl vapor-induced corrosion at 650 °C in static air. Both elements were found to have a positive effect in reducing corrosion with silicon showing a superior beneficial effect compared to aluminum. In a similar study within the same research group, iron, chromium and a range of iron-chromium alloys along with their aluminum/silicon modifications were evaluated at 650 °C under air+KCl deposit. A positive effect on the corrosion resistance was observed with aluminum or silicon additions [4].

The mechanism of alkali chloride-induced high temperature corrosion is still a subject of discussion. Pettersson et al. [2] showed that the presence of potassium is enough to cause breakdown of the initial chromium-rich protective oxide on chromia-forming alloys due to the formation of potassium chromate (K_2CrO_4). *Lehmusto* et al. [15,16] investigated the corrosion behavior of selected chromia-forming alloys under either KCl or K_2CO_3 and found both salts corrosive. In another study within the same research group it was found that when pure chromium is exposed to either KCl or K_2CO_3, the presence of potassium alone could initiate the attack, while chloride was necessary for the reaction to continue [11].

The present paper is the second part of a larger study evaluating the performance of a wide range of commercial alloys. In the first part [17] selected chromia-forming alloys failed to form a protective oxide layer when KCl was present, either as a salt or as a gas. The formed oxide on stainless steels consisted of an outer part with a highly porous morphology (referred to as type A oxide) and an inner part which was apparently dense (referred to as type B oxide). For nickel-based alloys, type A oxide was always present. However, instead of an inner oxide as for the stainless steels, the nickel-based alloys sometimes exhibited deep-penetrating voids (indicative of selective corrosion) and/or pitting. This paper addresses the performance of selected chromia-forming alloys that contain aluminum or silicon. At the end, a complementary test was performed with either KCl or K_2CO_3 to obtain further understanding on corrosion mechanisms.

2 Experimental procedure

The chemical composition of the investigated alloys is given in Table 1. Samples were in the form of coupons (7-8 mm x 17-20 mm) with a thickness in the range of 250-340 μm. The samples were cut with a precision cutter. Alloy HR160 was delivered in rolled condition. For recrystallization the sample was annealed at 1150 °C for 45 min in Ar(g)(99.999% purity)+25vol. %H_2(g) followed by cooling in the furnace. Before annealing the sample was ground with 1000-grit SiC paper to remove solid surface contaminants.

Prior to exposure in a corrosive environment, all samples were ground with 4000 grit SiC paper and covered with a ~1 mm thick layer of KCl powder (particle size 63-90 μm) for ~2/3 of their length. Samples were placed on flat alumina coupons and then loaded into a multi-channel alumina sample holder with the KCl-free part towards the entrance of the gas flow. The sample holder itself was then placed in the zone of uniform temperature in a silica tube in the horizontal furnace. A schematic representation of the experimental set-up is shown in Figure 1.

Exposures were conducted at 600 °C for 168 h. The gaseous atmosphere consisted of flowing N_2(g)+5%O_2(g)+15%H_2O(g)

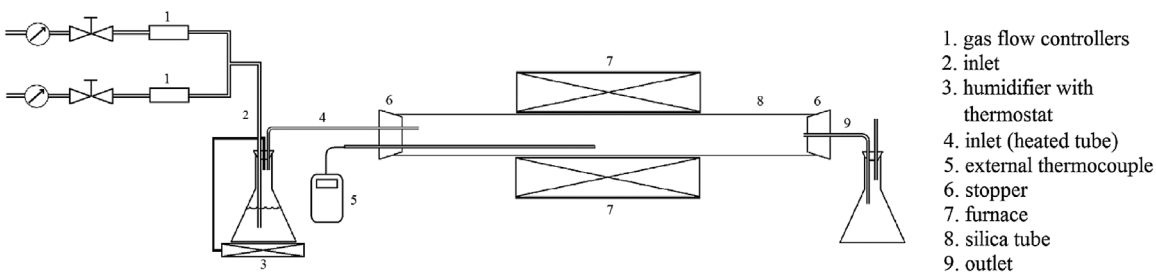

Figure 1. Schematic of the experimental set-up

with a calculated velocity of 0.25 cm/s at the inlet temperature. An exposure without salt was performed for all of the alloys as a reference test. For alloy HR160 the exposure with salt was repeated. In this second run, the sample was ground with 1000 paper prior to grinding with 4000 paper. This was undertaken to remove any possible oxide formed during annealing. To distinguish between the two samples, the one ground with only 4000 paper is referred to as series 1 and the sample ground with, 1000 and then 4000 paper is referred to as series 2. In addition to the above-mentioned exposures, one extra test was performed with Nimonic 80A where one sample was covered with KCl and the other with K_2CO_3 of the same particle size. Samples were separately exposed at 600 °C for 168 h. As the K_2CO_3 is deliquescent, this test was performed in static lab air to avoid formation of a liquid phase during the purging period of the furnace.

After the exposures, KCl-exposed samples were clamped in an upright position and embedded in epoxy resin without removing the salt layer. For the K_2CO_3-exposed sample, the salt layer spalled off after the test, therefore only the sample was embedded. Half the width of the embedded samples was removed by grinding with 180-grit SiC paper and then grinding/polishing was continued on finer paper/cloth grades down to 1 μm diamond suspension. As lubricant, 96% ethanol was used for grinding up to the 1000-grit paper and 99.9% ethanol on finer papers. Since chlorine was detected in the original epoxy (specifix-20), a chlorine-free epoxy (Eli-Cast clear epoxy) was used for the series 2 sample of alloy HR160. In addition, one exposed (series 2) sample of this alloy was thoroughly washed with de-ionized water after the test to remove the water soluble corrosion products. Phase analysis of the samples of the reference exposure (i.e. the KCl-free exposure) were performed with an X-ray diffractometer (Bruker D8 Discover). CrK_α (λ=2.2897 Å) radiation was applied in grazing incidence mode to limit the information depth of the applied radiation and thus investigate the surface adjacent region of the samples. Due to the incorporation of corrosion products into the residual salt layer, removal of the salt without unintentional removal of the corrosion products proved to be challenging. Therefore KCl exposed samples were not investigated with XRD. Reflective light microscopy (RLM) was used to measure the decrease in metal thickness for the salt-affected samples. Twenty measurements were done at intervals of 0.5 mm. The average and standard deviation were calculated for each sample based on these measurements. Subsequently, the entire surface was thoroughly inspected to find the worst case damage. Average and worst case values less than 5μm were considered insignificant, considering the accuracy of the micrometer employed for pre-exposed sample thickness measurements. The morphology of corrosion and elemental distribution in the corrosion products were investigated by means of an FEI Inspect S scanning electron microscope (SEM) equipped with an energy dispersive X-ray spectroscopy (EDS) detector. Image acquisition was always performed in back-scattered electron (BSE) mode. The chemical compositions of the alloys as listed in Table 1 were measured with EDS. Carbon and nitrogen contents were measured with fusion thermal conductivity detection units LECO CS230 and LECO TN500 respectively.

3 Results

3.1 Reference exposure in $N_2(g)+5\%O_2(g)+15\%H_2O(g)$

After the salt-free exposure in $N_2(g)+5\%O_2(g)+15\%H_2O(g)$, only the austenitic stainless steel 153MA developed a fast growing oxide. A dull-red colored oxide had developed on the surface and the cross section revealed a double layer oxide (Figure 2). For the other alloys, no oxide was observed on visual inspection and the metallic luster was preserved. Corresponding diffractograms are given in Figure 3. For alloy HR160 the diffractogram corresponds to a series 1 sample. The precipitate phases were identified as Ni_3Al for alloy 214 and $Cr_{23}C_6$ for 153MA. For 153MA, peaks belonging to $(Fe,Cr)_2O_3$ and $(Fe,Cr)_3O_4$ can be clearly distinguished. For the other alloys, no indication of a fast-growing oxide was observed.

3.2 Exposure in $N_2(g)+5\%O_2(g)+15\%H_2O(g)$ under KCl(s)

Although the majority of the alloys formed protective oxides in the salt-free exposure, they all suffered from significant corrosion under a KCl deposit. Figure 4 shows the reduction in metal thickness for the investigated alloys. As TP347HFG is the alloy currently utilized for superheater materials in many biomass fired plants, the result for this alloy (taken from the first part of this study [17]) is included for comparison. In addition to the general thickness loss, internal oxidation, grain boundary attack and void formation are also included as part of the reported decrease in metal thickness. Considering both average and worst case measurements, none of the alumina-forming alloys performed better than TP347HFG. For Alloy 214, the average thickness loss is lower than for TP347HFG, however localized thickness loss is higher. For the two silica-forming alloys, 153MA does not show any improvement compared to TP347HFG while it is indicated that the nickel-base alloy HR160 shows a slightly

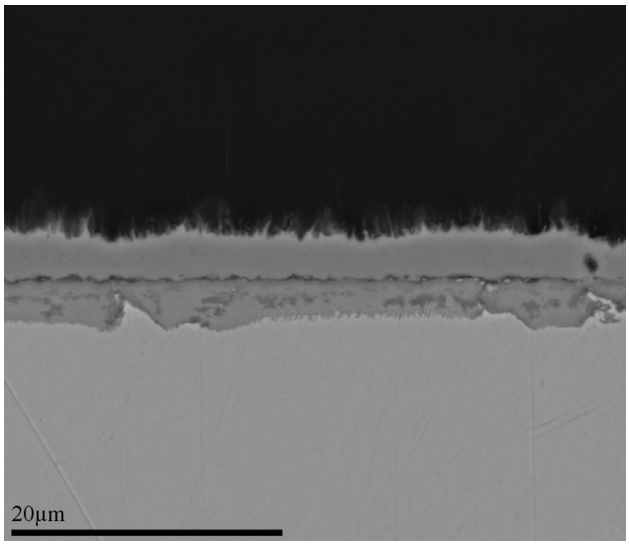

Figure 2. Oxide morphology observed on 153MA due to the exposure in N2(g) + 5%O2(g) + 15%H2O(g) at 600 °C

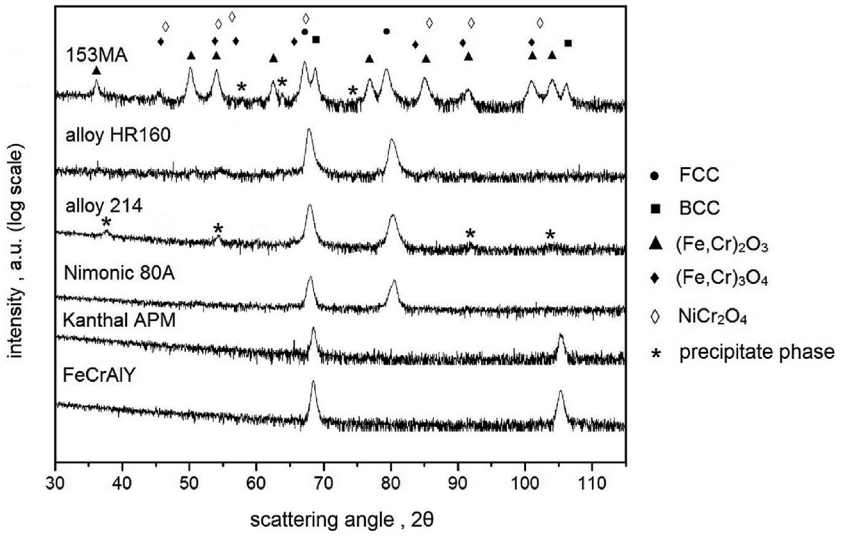

Figure 3. CrKα X-ray diffractograms for the investigated alloys after the salt-free exposure. The angle of incidence has been between 1-5 degrees

better performance. The value reported for HR160 in Figure 4 is for a series 2 sample, but no significant difference between series 1 and 2 samples of the alloy could be found. Corrosion morphologies and EDS mapping of the corrosion products for different alloys are reported in the following sections.

3.2.1 Alumina-formers

3.2.1.1 FeCrAlY and Kanthal APM: The microstructure of the corrosion products on FeCrAlY and Kanthal APM showed many similarities (Figures 5a-b). For both FeCrAlY and Kanthal APM, two distinct oxide morphologies (referred to as type A and type B) were observed, similar to the stainless steels mentioned in the first part of this study [17]. The cavities in the epoxy are the locations where salt particles were grazed-out during grinding for sample preparation. The outermost oxide (type A) was voluminous showing considerable porosity. This oxide was rich in iron and also contained aluminum and chromium (Figures 6 and 7). Minor amounts of potassium could be detected in this oxide too. The type B oxide, located underneath the type A oxide, was relatively dense and was rich in chromium and aluminum, showing aluminum enrichment with depth. The type B oxide was often locally extended deep into the alloy, presumably along alloy grain boundaries. Underneath the type B oxide, a region was observed with darker contrast compared to the matrix and brighter contrast compared to the oxide. Spot analysis revealed the presence of oxygen throughout this region indicating an internal oxidation zone (IOZ). This zone was thicker for FeCrAlY than for Kanthal APM. Chromium depletion was observed for both alloys in the IOZ. The high chromium content found at the tip of the grain boundary in Figure 7 is suggested to be a chromium carbide particle lying at this location. Similar high chromium locations were also observed in the unexposed microstructure of Kanthal APM. Spot analysis revealed that the thin dark line separating the IOZ from the unaffected alloy is slightly enriched in nitrogen and aluminum. Below this dark

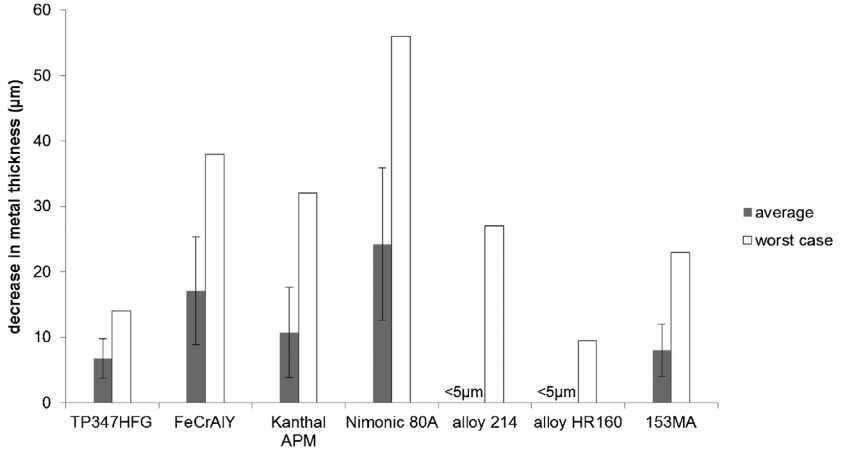

Figure 4. Average and highest thickness loss observed on the studied alloys after 168 h exposure at 600 °C in N2(g) + 5%O2(g) + 15%H2O(g) under KCl(s). TP347HFG is included from [17] for comparison

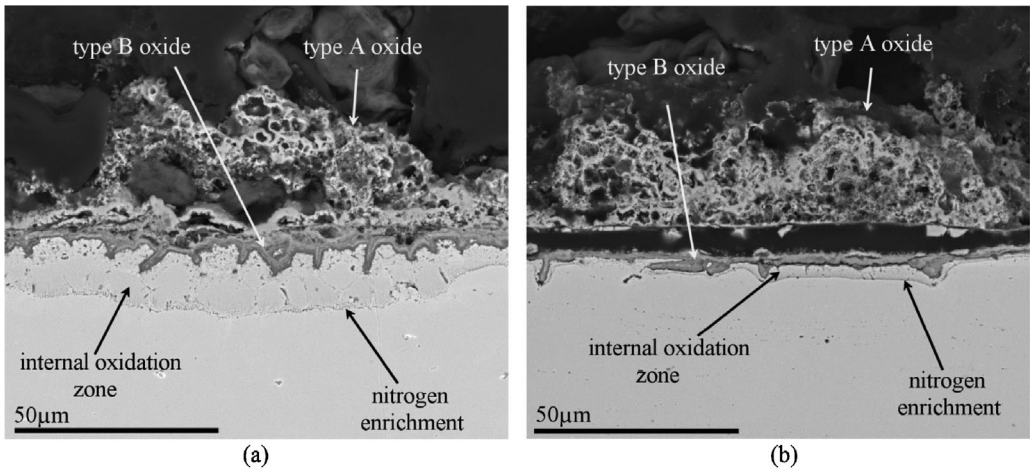

Figure 5. General corrosion morphology on (a) FeCrAlY and (b) Kanthal APM showing grain boundary attack and internal oxidation

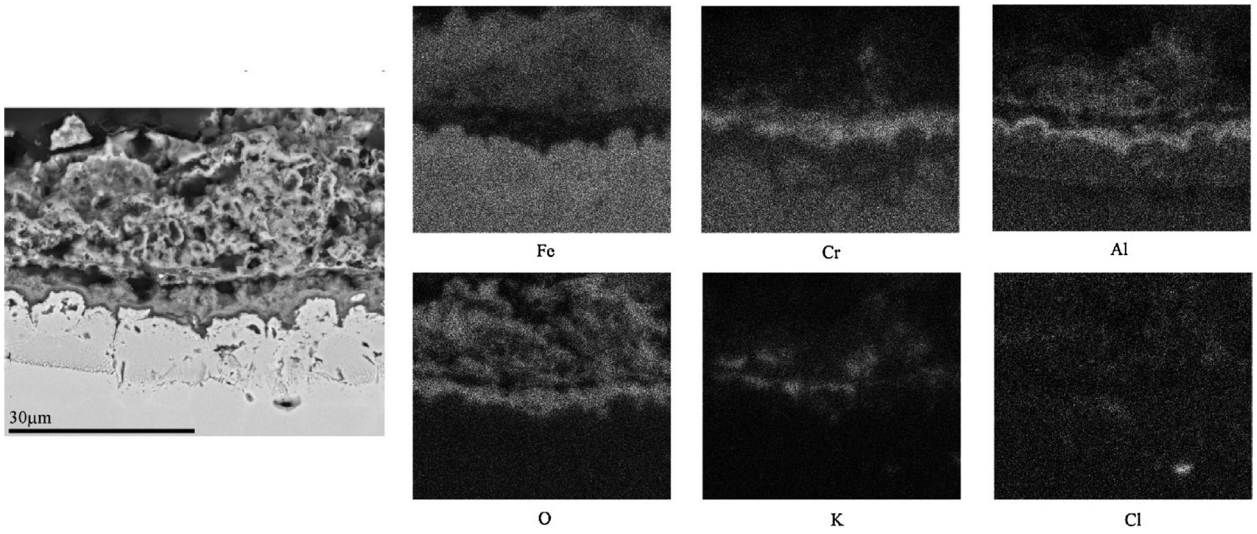

Figure 6. Distribution of the alloying elements, potassium, chlorine and oxygen in the corrosion product developed on FeCrAlY

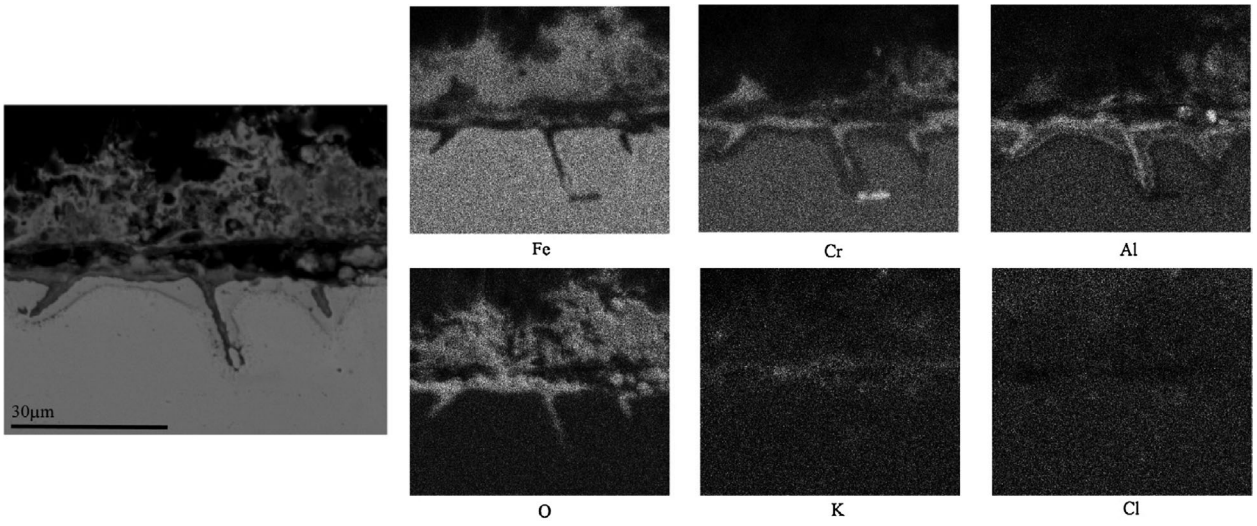

Figure 7. Distribution of the alloying elements, potassium, chlorine and oxygen in the corrosion product on Kanthal APM

line, aluminum depletion is observed. In a number of cases, potassium and/or chlorine could be found in the type B oxide, in the IOZ and even at the metal/IOZ interface. It is not clear whether this is a real effect or an artefact of the polishing process, for example by smearing these species over the surface.

3.2.1.2 Nimonic 80A and Alloy 214: For Nimonic 80A, the corrosion products consisted of a spongy oxide containing chromium, aluminum, titanium and potassium with minor amounts of nickel (Figures 8a-c). This oxide was highly porous and voluminous (see Figure 8a) and thus had the same characteristics as the type A oxide observed on the investigated stainless steels reported in [17] and FeCrAlY/Kanthal APM. No clear sign of chlorine enrichment could be seen in the corrosion morphology. The outer parts of the spongy oxide showed a eutectic-looking structure (Figure 8b) with strips embedded in a potassium-chromium-oxygen compound suggesting a solidification product. Alloying elements were found at distances more than 100 μm away from the original metal surface, see Figures 8b-c. Beneath the spongy type A oxide, a porous metallic zone was observed. This zone was enriched in nickel and depleted in chromium, aluminum and titanium. In some cases the nickel skeleton was absent, indicating that even nickel had been attacked (see the cavity marked in Figure 8c). A ~1-2 μm thin layer separates the porous nickel-rich alloy from the spongy corrosion product (see aluminum, titanium and chromium map in Figure 9). A titanium-rich phase could be found in the bulk alloy microstructure (marked with dashed arrows in Figure 8a). EDS spot analysis indicated the presence of nitrogen in this phase, therefore it is assumed to be titanium nitride. Interestingly, the particle with dark contrast in the porous nickel-rich zone (Figure 8a) seems to be intact, which suggests that this phase has not been significantly attacked. In addition to the titanium-rich phase, a chromium-rich phase, likely to be carbides, was found at many locations in the microstructure (marked with solid short arrows in Figure 8a).

Alloy 214 showed a unique behavior. On most of the surface, no significant thickness loss (<5 μm) was observed and a dense uniform nickel-rich band of 4-5 μm was present (see the bright contrast close to the surface in Figure 10a). What appears to be a thin aluminum and chromium-rich oxide could be observed over the entire surface (see aluminum map in Figure 11). There were only two areas along the 12 mm long specimen where localized attack and porous nickel rich areas could be found (Figure 10b).

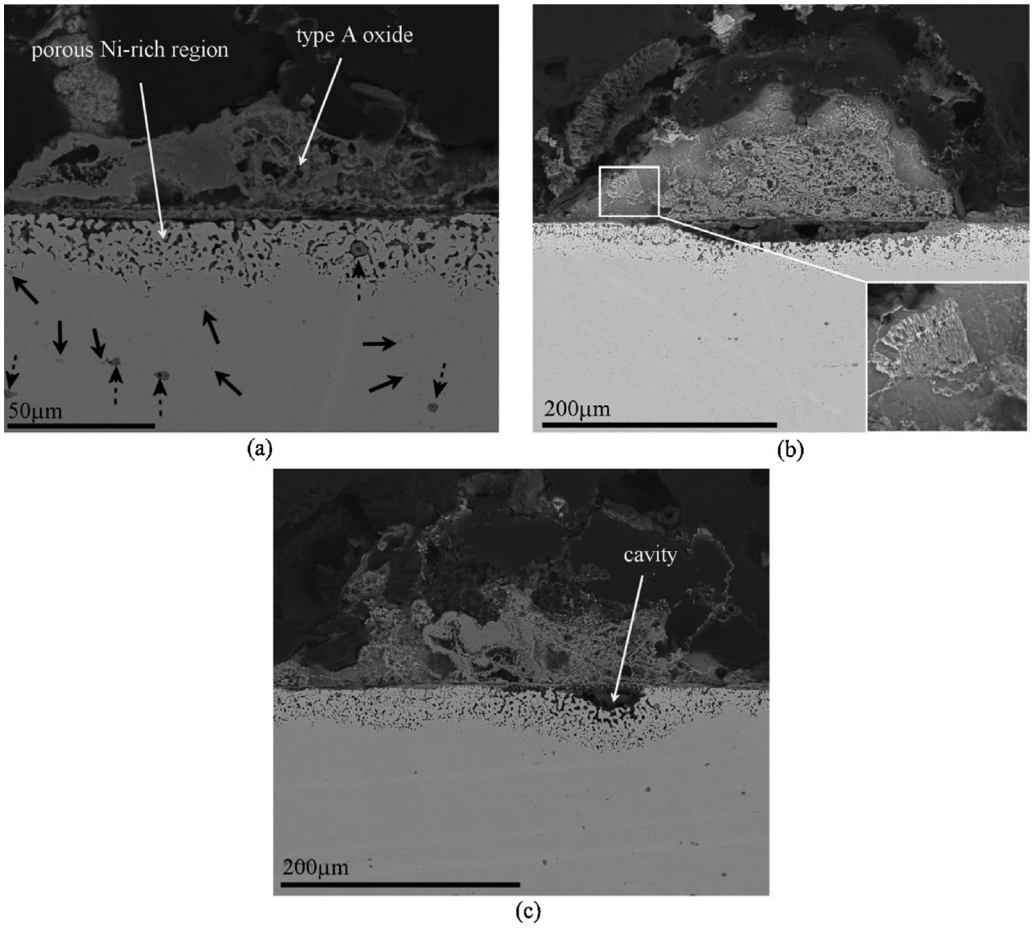

Figure 8. General morphology of corrosion products on Nimonic 80A. (a) Dashed short markers denote the titanium nitride and the solid short markers denote the chromium-rich phase in the bulk. (b) Eutectic structure of the outer corrosion products (higher magnification in inset). (c) Depressions in the alloy indicate that even nickel has been attacked locally

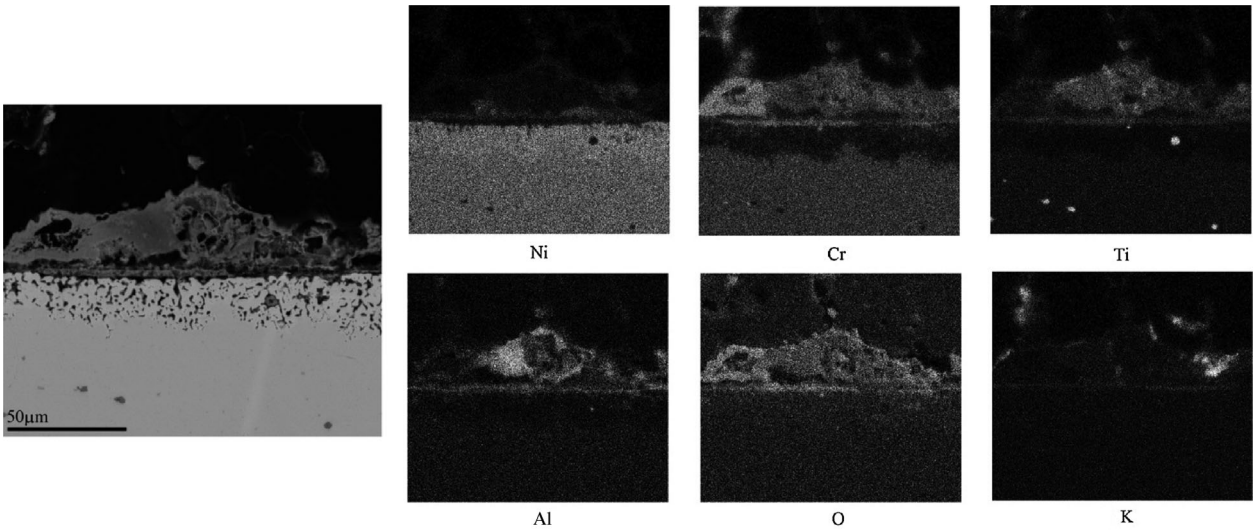

Figure 9. Distribution of the alloying elements, potassium and oxygen in the corrosion product on Nimonic 80A

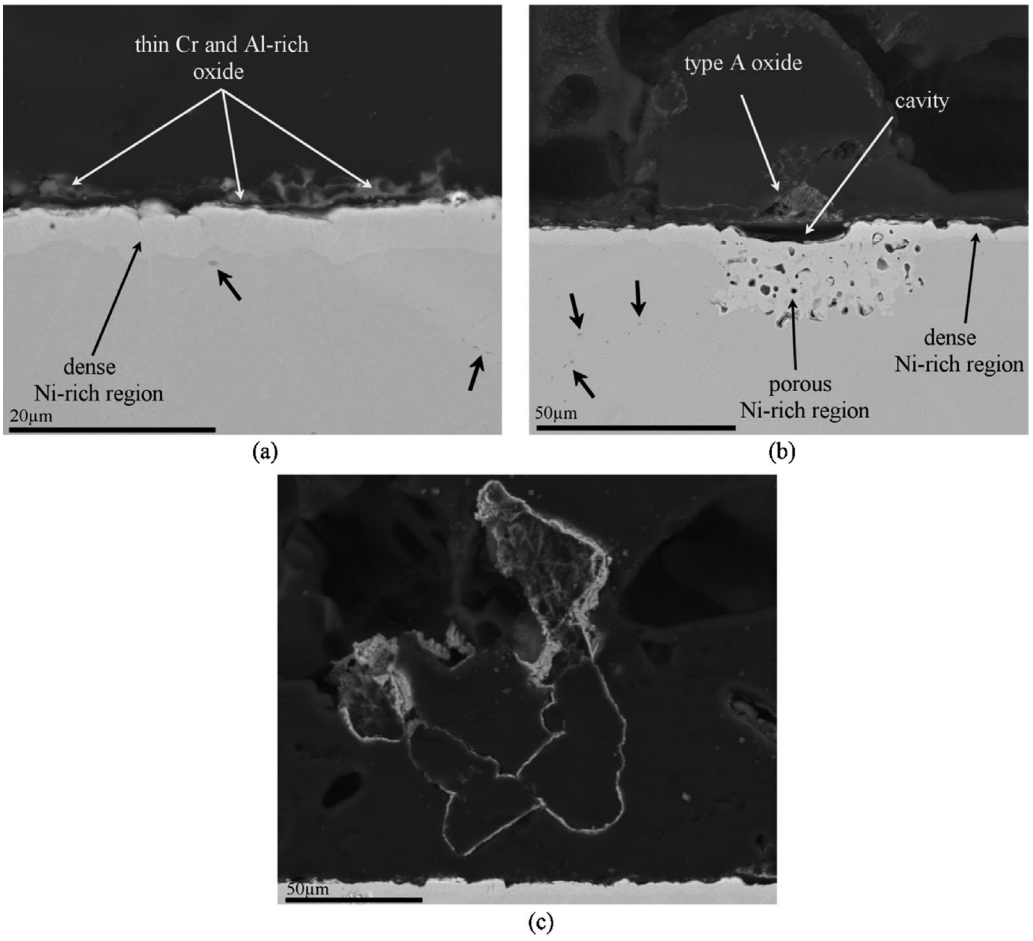

Figure 10. Corrosion morphologies on alloy 214. (a) Large parts of the surface show a dense nickel-rich band. Short arrows denote the chromium-rich phase, (b) local attack of the alloy in the form of selective corrosion, (c) bubble-like oxides reach far into the KCl deposit

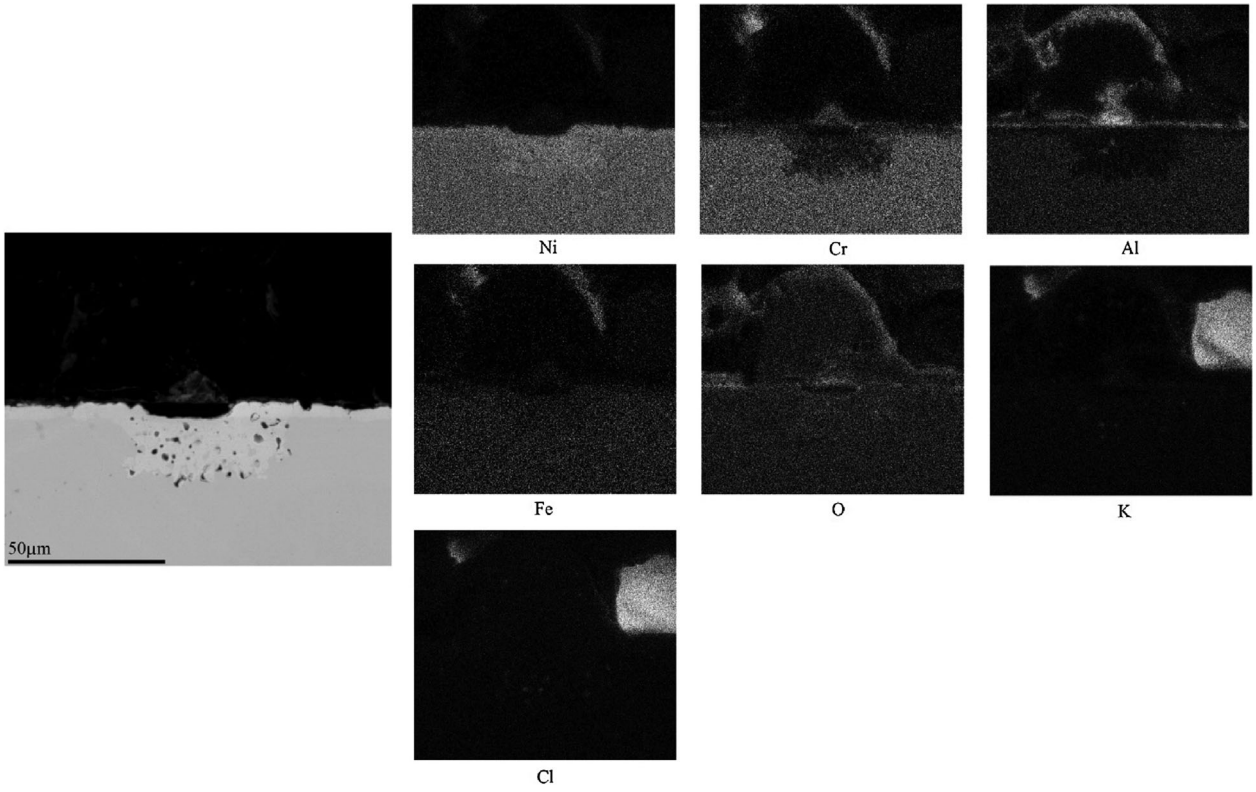

Figure 11. Distribution of the alloying elements, potassium, chlorine and oxygen in the corrosion product on alloy 214

EDS mapping and spot analysis of these porous areas showed strong nickel-enrichment and aluminum/chromium depletion similar to the general behavior observed on Nimonic 80A. In addition, detection of nickel in the oxide as well as a cavity underneath the oxide suggests that even nickel was removed. EDS mapping of the spongy oxide above the two deep nickel-rich areas showed a mixture of aluminum, chromium and iron oxides with a small amount of nickel (Fig 11). A chromium-rich phase could be seen in the microstructure (marked with short arrows in Figures 10a and b). In addition to the unreacted KCl, a faint enrichment of both potassium and chlorine can be seen in the spongy nickel-rich area. However, it is not clear if this is a real effect or an artefact of polishing. Bubble-like oxides extending more than 100 μm away from the corrosion front were often observed (Figure 10c). The selective nature of corrosion as well as the presence of a voluminous and highly porous oxide was similar to Nimonic 80A.

3.2.2 Silica formers

3.2.2.1 153MA: Similar to the stainless steels considered in the first part of this study, the morphology of corrosion products on 153MA consisted of type A and type B oxides (Figure 12). The higher Si content of 153MA (1.6 wt%) compared to the other investigated stainless steels, did not appear to have a significant effect on the behavior of this alloy. The distribution of the alloying elements throughout the corrosion product is shown in Figure 13. The type A oxide was rich in iron and contained a small area where potassium and chromium were both present. The outer type B oxide was iron rich above the assumed original metal surface and chromium rich below this interface; there were also indications of silicon enrichment at the presumed original surface and within the inner part of type B oxide together with chromium. Metallic islands enriched in iron and nickel were also identified. No clear chlorine enrichment was detected.

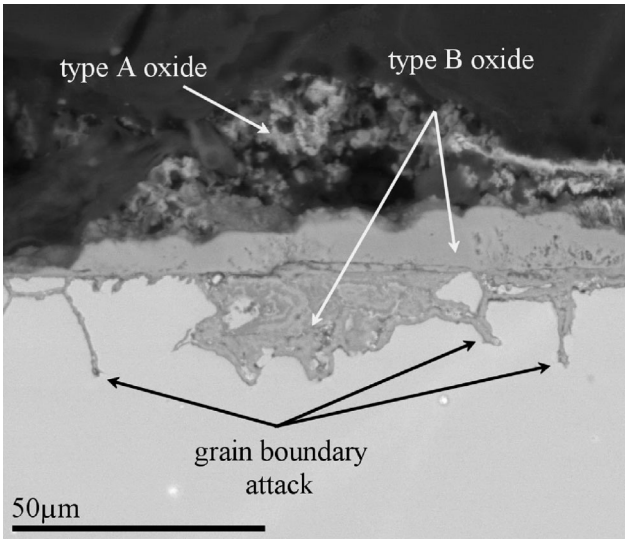

Figure 12. General corrosion morphology observed on 153MA

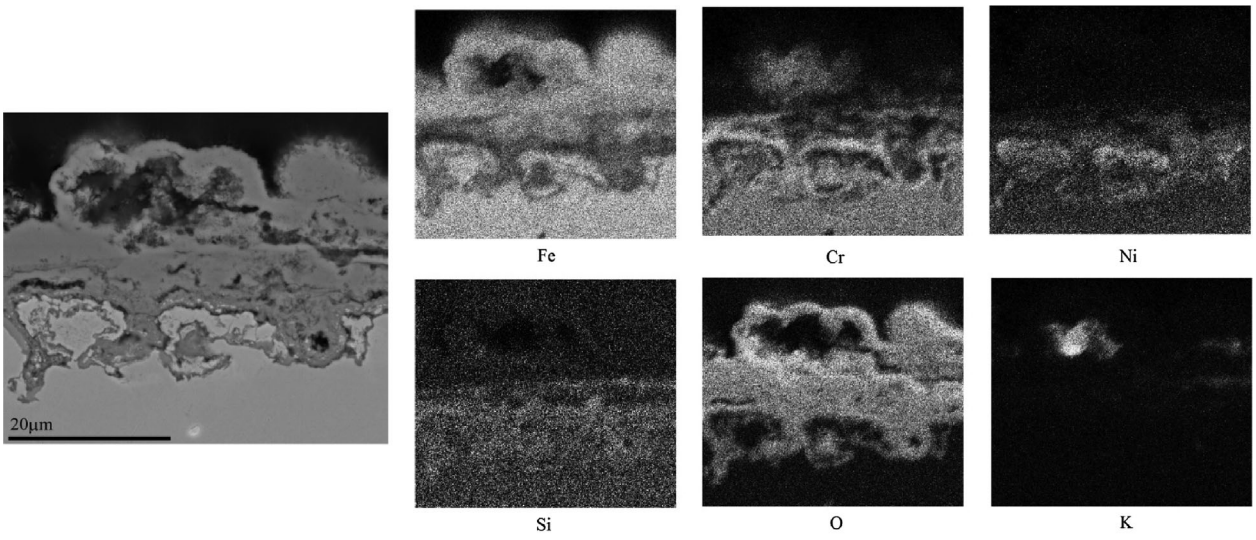

Figure 13. Distribution of the alloying elements, potassium and oxygen on 153MA

3.2.2.2 Alloy HR160: Alloy HR160 shows similar corrosion morphology as type A and type B oxides for both surface qualities (series 1 and 2). Type A oxide was composed of spongy cobalt and nickel-rich oxides mixed with large amounts of a potassium-chromium-oxygen containing compound. Type B oxide is rich in nickel and cobalt on the top (at the presumed original metal surface) and consists of a potassium-silicon-chromium-oxygen type compound (or mixture of compounds) below this (Figures 14 and 15). No clear enrichment of chlorine was observed. In a few cases the corrosion product showed a shallow penetration into the alloy, presumably along grain boundaries (Figure 14). Examination of the sample that was rinsed with de-ionized water showed that potassium was not removed from the type B oxide by washing, indicating that potassium is not present as a water soluble compound. A nickel and cobalt-rich band could be observed below the corrosion front together with depletion of chromium and silicon, but void formation in this band was very rare. Titanium was present as needle-like precipitates within the alloy close to the surface (marked with short arrows in Figure 14). However, these precipitates were present in the microstructure of the unexposed alloy as well and are therefore not a result of the exposure. EDS spot analysis showed that nitrogen was present in these precipitates i.e. titanium nitride was found in the microstructure close to the surface.

3.3 Comparison between KCl and K_2CO_3 on Nimonic 80A

The morphology of corrosion products on Nimonic 80A exposed in static lab air under KCl(s) was quite similar to the exposure in flowing N_2(g)+5%O_2(g)+15%H_2O(g) under KCl(s). However, replacing KCl by K_2CO_3 resulted in a significant change in the corrosion product morphology. No highly porous outermost oxide (type A oxide) was found, neither was a eutectic-looking mixture identified after exposure with K_2CO_3. Moreover, no voids were detected in the metal above the corrosion front. The distribution of the alloying elements showed inner and outer corrosion products for the K_2CO_3 exposure (Figure 16a). The outer corrosion product was rich in nickel, while nickel was depleted in the underlying alloy. Moreover, the EDS spot analysis and the very bright contrast of the outer corrosion product in Figure 16a indicated the presence of metallic nickel in the outer layer. The nickel denuded region has higher chromium and higher oxygen content; these observations combined with the dark contrast in the BSE image in Figure 16a is ascribed to internal oxidation of chromium. In contrast, the KCl-affected sample displays a morphology where chromium is removed and nickel is enriched in the alloy (Figure 16b). The nickel-rich area showed development of porosity deep into the alloy.

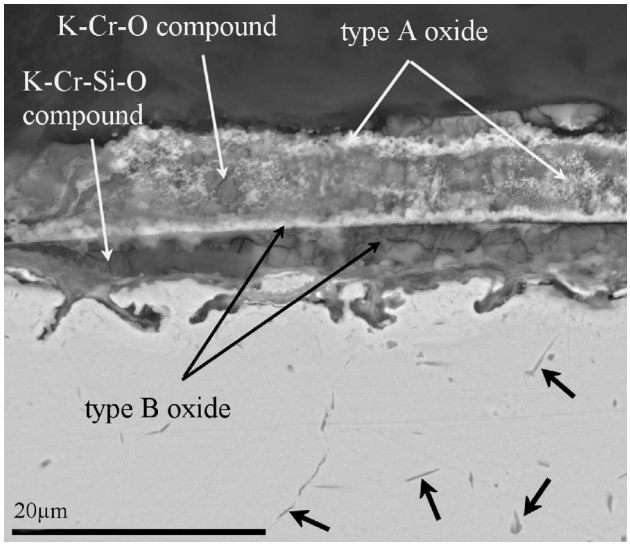

Figure 14. General corrosion morphology observed on alloy HR160. Short arrows indicate a titanium-rich phase

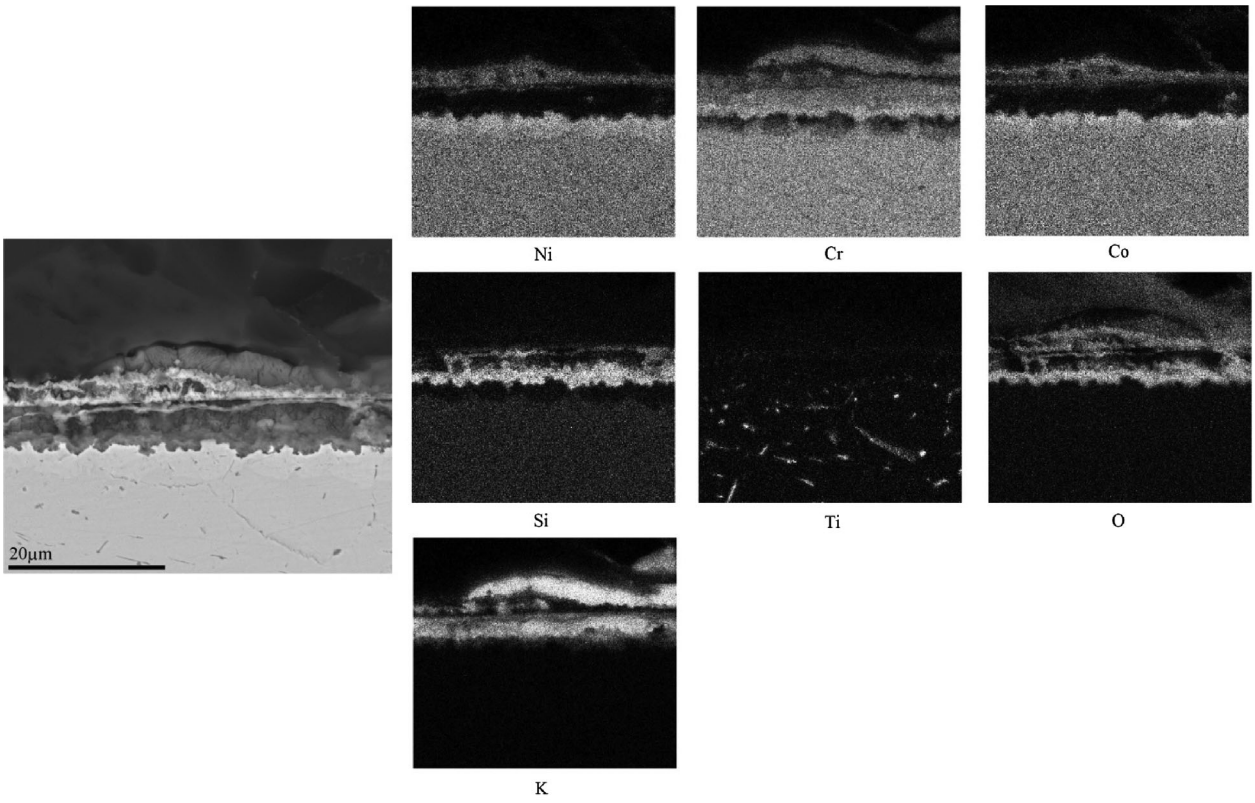

Figure 15. Distribution of the alloying elements, potassium and oxygen in the corrosion product on alloy HR160

4 Discussion

4.1 Reference exposure in $N_2(g)+5\%O_2(g)+15\%H_2O(g)$

It has been indicated that for alloys relying on chromia for protection, evaporation of chromium from the oxide in the form of chromic acid, $CrO_2(OH)_2$, induces breakdown of chromium oxide in humid-oxidizing conditions [18,19]. Accordingly, the protective capacity of the oxide layer depends on a balance of the rates of chromium depletion by evaporation and chromium replenishing by supply from the substrate. Alumina and silica are less volatile than chromia in humid-oxidizing environments and therefore aluminum and silicon form protective oxides [20]. However, due to the limited solubility of aluminum and silicon in iron and nickel, formation of a protective alumina or silica layer on a binary solid solution of iron or nickel with silicon or aluminum under humid-oxidizing conditions is not expected; rather internal oxidation of these elements would be anticipated. Therefore an initial chromia layer is necessary to retard the oxygen ingress so that diffusion of aluminum or silicon to the oxidation reaction front can proceed faster than diffusion of oxygen into the alloy; the so called "third element" effect [21]. Hence, alumina or silica can develop underneath a chromia layer and, consequently, the resistance of alumina and silica-forming alloys is, at least partly, dependent on the chromium content and/or the supply of chromium to the surface. Under the experimental conditions of this study, only the stainless steel 153MA (containing 21.3at% Cr) does not satisfy this condition. Apparently, for this alloy the flux of chromium to the surface is insufficient to maintain the chromia layer. Consequently no protective silica layer forms on this alloy. A chromia layer is formed for the other alloys where the Cr content was evidently of an adequate level at 22.2-30.8 at.%. However, alloy 214 has only 18 at.% Cr so in that case, the 9.7 at.% Al must have contributed to the formation of the initial oxide layer. This hypothesis is supported by the fact that alumina has some solubility in chromia therefore it can contribute to the formation of a protective oxide at a very early stage of oxidation.

4.2 Exposure in $N_2(g)+5\%O_2(g)+15\%H_2O(g)$ under KCl(s)

In contrast with the salt-free exposure, where the majority of the investigated alloys showed passive behavior, all alloys suffered from significant attack when KCl was present. This shows that none of the studied alloys is able to form a protective oxide during the early stages of the attack. This effect is attributed to the presence of potassium reacting with chromia to form potassium chromate and thus acting as a chromium sink [2]. In this respect, water vapor and oxygen have a synergy with potassium in removing chromium from the oxide layer. However, *Jonsson* et al. [22] showed that even under dry conditions at 600 °C the presence of a small amount of KCl suffices to locally break down the protective chromium-rich oxide on stainless steel 304L (Fe18Cr10Ni wt%). Further discussion for the different alloys is given in the following sections.

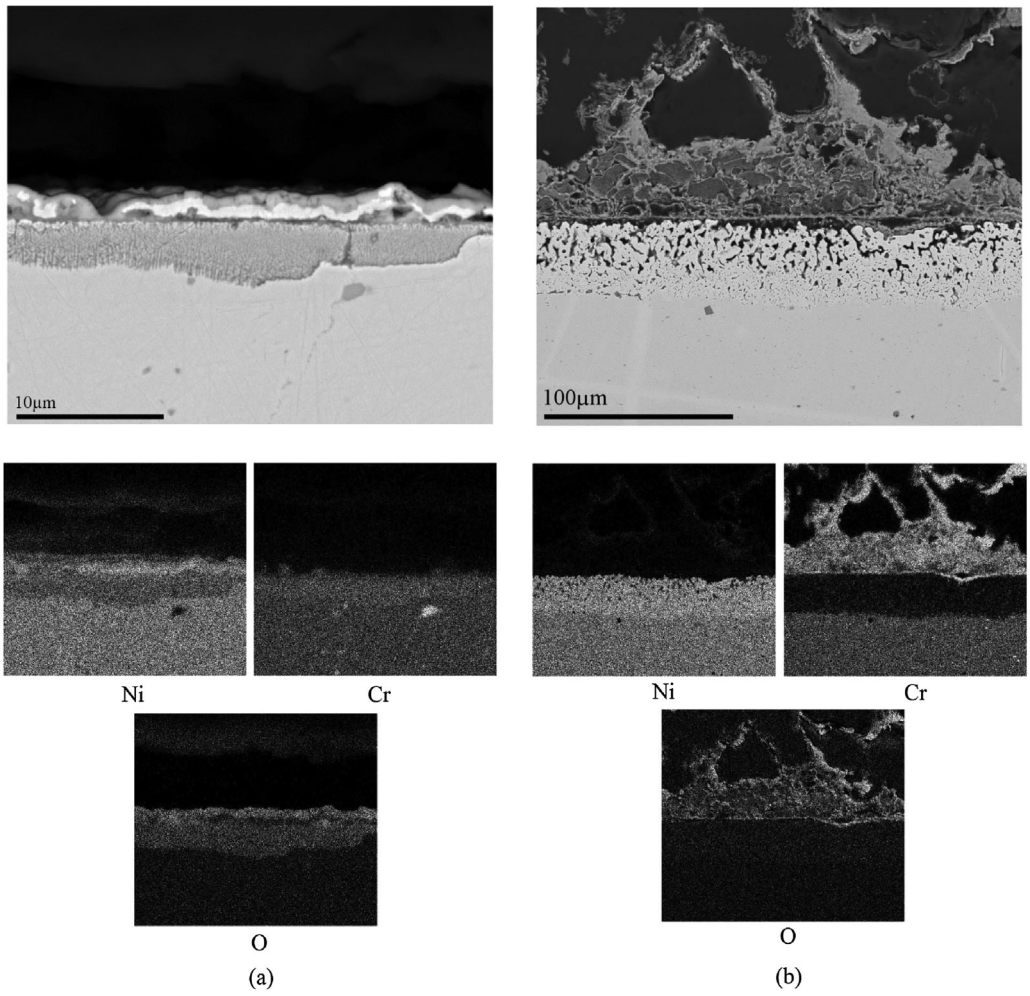

Figure 16. Comparison between corrosion morphologies on Nimonic 80A after exposure to (a) K2CO3 and (b) KCl. The distribution of nickel, chromium and oxygen is shown below the corresponding micrograph

4.2.1 Alumina formers

4.2.1.1 FeCrAlY and Kanthal APM: FeCrAlY and Kanthal APM exhibited both the outer porous type A oxide and the more dense type B inner oxide. In addition an internal oxidation zone was present for both alloys at the corrosion front. The difference in the morphology of type A and type B oxides strongly suggests that the mechanisms contributing to the formation of these oxides are different. The highly porous structure of type A oxide and the presence of potassium in it suggests the presence of a molten phase at some stage during the exposure. In high temperature corrosion the formation of a molten phase due to alkali chlorides has often been reported [23–27]. For pure iron and low alloy steel, a molten phase is believed to form from $FeCl_2$ and unreacted KCl with a eutectic temperature of 355 °C [24]. If $FeCl_2$ does not evaporate, it will subsequently oxidize as it is metastable at the oxide/gas interface. The presence of aluminum in type A oxide shows that it is incorporated into the oxide in a similar way as iron and, hence, does not always contribute to a protective layer. The dense appearance of the type B oxide, on the other hand, suggests that it has formed due to solid state diffusion of ions in a dense crystalline lattice. However, the formation of an internal oxidation zone (IOZ) underneath type B oxide shows that it is not an effective diffusion barrier. These findings indicate that oxygen is supplied faster to aluminum in solid solution than aluminum to the oxidation front leading to the formation of an IOZ. In addition, the aluminum enrichment in the lower part of the type B oxide does not offer sufficient protection against the inward diffusion of oxygen (and nitrogen). This is in agreement with the study by *Zahs* et al. [28] where it was found that on Fe-15Cr-5Al (wt%) exposed to N_2(g)-5%O_2(g) at 600 °C, only γ-alumina forms within 168 h. The γ polymorph of alumina is not desired as it is often believed that only the α-alumina, which forms at higher temperatures, is slow-growing i.e. protective [21]. The superior performance of TP347HFG compared to FeCrAlY/Kanthal APM shows that the presence of aluminum in Fe-Cr solid solutions under the present low temperature humid-oxidizing conditions leads to a larger reduction in metal thickness due to internal oxidation than an aluminum-free alloy. In this case the presence of aluminum does not promote the formation of a protective oxide layer. This has also another outcome: nitrogen enrichment underneath the IOZ can lead to the formation of aluminum nitride. The nitrogen involved in the formation of nitrides most likely originates from (reactions with) the carrier gas N_2(g);

alternatively it can be the result of the dissolved nitrogen in the alloy that is pushed ahead of the internal oxidation front.

Observation of similar features for FeCrAlY and Kanthal APM can be attributed to a general similarity in composition. The result in Figure 4 indicates a slight difference between the two, which originates from a thicker IOZ for FeCrAlY compared to Kanthal APM. This can be due to a smaller grain size for FeCrAlY (ASTM no 10) compared to Kanthal APM (ASTM no 7). If a protective oxide fails to form, grain boundaries may act as a preferential oxygen "inlet" and therefore a thicker IOZ will form.

4.2.1.2 Nimonic 80A and Alloy 214: The morphologies of the corrosion products on Nimonic 80A and alloy 214 are similar to type A oxide observed on the stainless steels. This suggests that these oxides are formed from oxidation of metal chlorides. Even though the oxide on both nickel-base alloys is chromium and aluminum-rich, it is highly porous and not protective. Apparently the presence of aluminum (and even chromium) in the alloy has not been beneficial as preferential removal of the alloying elements leads to a porous alloy consisting of Ni. The observation that only highly electropositive elements as chromium, aluminum and titanium have been removed from the alloy shows that a selective corrosion mechanism causes the attack, This is most likely due to a chlorination-evaporation-oxidation sequence. Selective removal of chromium, aluminum and titanium and rather passive behavior of nickel can be described in terms of relative thermodynamic stability of the alloying elements' chlorides [29].

Comparing Figures 8a and 10b, it is obvious that Nimonic 80A is attacked more severely by chlorination than alloy 214, since a porous nickel enriched band is observed uniformly along the surface of Nimonic 80A, while it occurs only locally for alloy 214. A straightforward explanation for this difference cannot be given on the basis of the results obtained and further investigation is necessary.

4.2.2 Silica formers

4.2.2.1 153MA: The content of 1.6 wt% (3.1 at%) silicon in this alloy did not result in a significant difference compared to low-silicon stainless steels of comparable chromium and nickel contents (TP347HFG and TP347H). As no regions with a contrast darker than the metal and brighter than the oxide in the BSE images (similar to that observed on FeCrAlY/Kanthal APM) were found, this indicates that no internal oxidation/nitridation of silicon has occurred.

4.2.2.2 Alloy HR160: The corrosion product on alloy HR160 is largely composed of potassium, chromium, silicon and oxygen (Figure 16). This is consistent with previous observations that chromia and silica react with KCl in an oxygen containing environment [30]. Limited thickness loss on this alloy (Figure 4) indicates that the corrosion product retards the progress of corrosion. Whether it is the higher chromium content, formation of a silica layer at the metal/oxide interface or the potassium-chromium-silicon-oxygen containing compound(s) itself that provides this protection requires further investigation. Since rinsing in water did not remove potassium, it is suggested that amorphous potassium silicate (or a mixture of silicates) has formed; amorphous potassium silicates are only slightly soluble in water at the ambient temperature [31]. The reason that the silicate does not form on 153MA may be due to the lower silicon content in 153MA compared to HR160, viz. 3.1 vs 6.5at.%.

In the first part of this study [17] it was shown that even infinitesimal amounts of oxygen and nitrogen impurities in the $Ar(g)+H_2(g)$ gas mixture used for annealing can cause oxidation and/or nitridation of alloys containing reactive oxide/nitride-forming elements such as aluminum or titanium. The presence of needle shaped titanium nitride particles close to the surface of alloy HR160 is attributed to such an effect. The fact that the annealing gas atmosphere had reacted with the sample surface may introduce inaccuracies to the result of the salt-free exposure. This is because a pre-formed oxide (silica or chromia+silica in case of alloy HR160) might have contributed to the passivation. However, since the series 1 sample was also attacked by KCl, the effect of a preformed thin oxide has been small (series 2 is ground with 1000 and 4000 papers, series 1 only 4000). In addition, the similar damage extent observed on both series 1 and 2 also discounts the presence of a thin oxide formed from annealing affecting the results. The lack of a significant protective effect from a preformed chromia and/or silica layer can be due to the reactivity of KCl with both silica and chromia [30].

4.3 Comparison between KCl and K_2CO_3 on Nimonic 80A

In the experiment with K_2CO_3, the formation of outer and inner corrosion products instead of a thin slow-growing oxide shows that the original protective oxide (chromia) on the alloy has been damaged. This can be explained by the reaction between K_2CO_3 and chromia leading to formation of potassium chromate (K_2CrO_4) [2,11,15,16,32]. Hence, the original diffusion barrier is lost and inward diffusion of anions coupled to outward diffusion of cations can take place leading to the formation of outer and inner corrosion products. However, a different morphology was observed after exposure of Nimonic 80A to KCl. Instead of oxygen ingress, the alloying element chromium, rather than the matrix element, is transported out of the alloy, leaving behind a porous nickel-rich skeleton. This demonstrates that chlorine can also play a role during high temperature corrosion where KCl is involved. The role of chlorine in accelerating the high temperature corrosion of metals and alloys is often ascribed to the volatilization of the alloying elements as their chlorides and oxychlorides [33–37]. Removal in form of subliming/evaporating chlorides is plausible for the current case as it explains void formation deep into the alloy. However, the exact mode of inward transport of chlorine and outward transport of species through the oxide layer requires further investigation.

5 Conclusions

From this study, the following conclusions can be drawn:

- Among the alloys Kanthal APM, FeCrAlY, Nimonic 80A, 214, HR160 and 153MA, only the 153MA formed a fast growing

duplex oxide within 168 h at 600 °C in N_2(g)+5%O_2(g)+15% H_2O(g). The presence of KCl led to extensive corrosion of all alloys.

- The presence of aluminum did not lead to the formation of a protective alumina layer on any of the investigated alloys exposed to N_2(g)+5%O_2(g)+15%H_2O(g)+KCl(s) at 600 °C. Based on a worst case criterion, under the experimental conditions of this study, none of the alumina-forming alloys showed less damage than the currently widely used material TP347HFG.
- The failure of aluminum to form a protective oxide on the iron-chromium and nickel-chromium alloys under the investigated conditions is due to a) aluminum chlorination and subsequent formation of alumina from oxidation of its chloride (alumina in type A oxide) and b) internal oxidation of aluminum (alumina under the type B oxide).
- The presence of 3.1 at% silicon in the austenitic stainless steel 153MA did not lead to a significant difference in performance compared to the low-silicon austenitic stainless steels with similar chromium and nickel content.
- On alloy HR160, a potassium-chromium-silicon-oxygen containing corrosion product was formed which seems to have a barrier effect against the continuation of corrosion. This alloy was the only alloy (among the ones addressed in this paper) that showed a better performance compared to TP347HFG.
- Both potassium and chlorine can play a role in the KCl-induced high temperature corrosion of chromia-forming alloys.

Acknowledgements: This work was performed within the framework of the project GREEN financed by the Danish Council for Strategic Research under grant number 10-093956. *Anette N. Hansson, John C. Troelsen, Flemming B. Grumsen* and *Peter J.S. Westermann* are acknowledged for their help and technical support during this work. Haynes® International is appreciated for supplying alloys 214 and HR160. Outokumpu is acknowledged for supplying stainless steel 153MA.

6 References

[1] M. Montgomery, S. A. Jensen, U. Borg, O. Biede, T. Vilhelmsen, *Mater. Corros.*, **2011**, *62*, 593
[2] J. Pettersson, H. Asteman, J. -E. Svensson, L. -G. Johansson, *Oxid. Met.*, **2005**, *64*, 23
[3] Y. Shinata, F. Takahashi, K. Hashiura, *Mater. Sci. Eng.*, **1987**, *87*, 399
[4] Y. S. Li, Y. Niu, M. Spiegel, *Corros. Sci.*, **2007**, *49*, 1799.
[5] M. Montgomery, A. Karlsson, *Mater. Corros.*, **1999**, *50*, 579.
[6] Y. Shinata, Y. Nishi, *Oxid. Met.*, **1986**, *26*, 201.
[7] Y. Shinata, *Oxid. Met.*, **1987**, *27*, 315.
[8] Y. S. Li, M. Sanchez-Pasten, M. Spiegel, *Mater. Sci. Forum*, **2004**, *461-464*, 1047.
[9] J. Lehmusto, D. Lindberg, P. Yrjas, B.-J. Skrifvars, M. Hupa, *Oxid. Met.*, **2011**, *77*, 129.
[10] J. Lehmusto, B.-J. Skrifvars, P. Yrjas, M. Hupa, *Corros. Sci.*, **2011**, *53*, 3315.
[11] J. Lehmusto, D. Lindberg, P. Yrjas, B.-J. Skrifvars, M. Hupa, *Corros. Sci.*, **2012**, *59*, 55.
[12] N. Hiramatsu, Y. Uematsu, T. Tanaka, M. Kinugasa, *Mater. Sci. Eng. A*, **1989**, 120-121, 319.
[13] H. Fujikawa, N. Maruyama, *Mater. Sci. Eng. A*, **1989**, *20*, 301.
[14] Y. S. Li, M. Spiegel, S. Shimada, *Mater. Lett.*, **2004**, *58*, 3787.
[15] J. Lehmusto, B.-J. Skrifvars, P. Yrjas, M. Hupa, *Fuel Process. Technol.*, **2013**, *105*, 98.
[16] J. Lehmusto, P. Yrjas, B.-J. Skrifvars, M. Hupa, *Fuel Process. Technol.*, **2012**, *104*, 253.
[17] S. Kiamehr, K. V. Dahl, M. Montgomery, M. A. J. Somers, *Mater. Corros*, **2015**, *66*, 1414.
[18] H. Asteman, J.-E. Svensson, L.-G. Johansson, *Oxid. Met.*, **1999**, *52*, 95.
[19] H. Asteman, J.-E. Svensson, M. Norell, L.-G. Johansson, *Oxid. Met.*, **2000**, *54*, 11.
[20] E. J. Opila, *Mater. Sci. Forum*, **2004**, *461-464*, 765.
[21] D. J. Young, *High Temperature Oxidation and Corrosion of Metals*, 1st ed., Elsevier, Amsterdam **2008**.
[22] T. Jonsson, J. Froitzheim, J. Pettersson, J.-E. Svensson, L.-G. Johansson, M. Halvarsson, in: *16th Int. Corros. Congr.*, Beijing, China, **2005**.
[23] N. Folkeson, T. Jonsson, M. Halvarsson, L.-G. Johansson, J.-E. Svensson, *Mater. Corros.*, **2011**, *62*, 606.
[24] T. Jonsson, N. Folkeson, J.-E. Svensson, L.-G. Johansson, M. Halvarsson, *Corros. Sci.*, **2011**, *53*, 2233.
[25] S. C. Cha, M. Spiegel, *Corros. Eng. Sci.*, **2005**, *40*, 249.
[26] S. C. Cha, M. Spiegel, *Mater. Corros.*, **2006**, *57*, 159.
[27] S. C. Cha, M. Spiegel, *Mater. Sci. Forum*, **2004**, *461-464*, 1055.
[28] A. Zahs, M. Spiegel, H. Grabke, *Mater. Corros.*, **1999**, *50*, 561.
[29] R. Bender, M. Schütze, *Mater. Corros.*, **2003**, *54*, 567.
[30] S. Kiamehr, K. V. Dahl, T. N. Lomholt, T. L. Christiansen, M. A. J. Somers: in: *Int. Symp. High Temp. Oxid. Corros. (ISHOC)*, Hakodate, Japan, **2014**.
[31] "soluble silicates", http://www.solublesilicates.eu/docs/solsil_broch_1302.pdf. [Accessed: 05-Sep-2014].
[32] J. Pettersson, N. Folkeson, L.-G. Johansson, J.-E. Svensson, *Oxid. Met.*, **2011**, *76*, 93.
[33] A. S. Kim, M. J. McNallan, *Corrosion*, **1990**, *46*, 746.
[34] J. M. Oh, M. J. McNallan, G. Y. Lai, M. F. Rothman, *Metall. Mater. Trans. A*, **1986**, *17*, 1087.
[35] M. H. Rhee, M. J. McNallan, M. F. Forthman, *J. Mater. Energy Syst.*, **1986**, *7*, 294.
[36] M. J. McNallan, *Mater. Perform.*, **1994**, *33*, 54.
[37] H. J. Grabke, E. Reese, M. Spiegel, *Corros. Sci.*, **1995**, *37*, 1023.

(Received: December 23, 2014) W8215
(Accepted: June 16, 2015)

